Semi-analytical model for the mechanical behavior of a spinning viscoelastic layer under gravity loads

Gérard-Philippe Zéhil
Faculty of Engineering
Notre Dame University - Louaize
P.O. Box: 72, Zouk Mikael, Lebanon
Email: gpzehil@ndu.edu.lb

***Abstract*—Recent works have proposed novel semi-analytical computational methods to model the viscoelastic rolling behavior of objects such as cylinders and spheres, including rolling resistance. This paper introduces and applies an extension of such methods to model the steady-state spinning behavior of a circular viscoelastic coating under the effect of gravity. The proposed modeling technique is wide-ranging in that it can accommodate any linear viscoelastic material characterized by its most general frequency-domain master-curves. The results of the model reveal that the mechanical behavior of the spinning viscoelastic coating is significantly different from that of a similar coating with purely elastic properties. The method can potentially be applied to characterize viscoelastic materials from either laboratory or field measurements. It could also be used to study the behavior of precision measurement devices and propellant grains under gravitational loads, or to model very large scale phenomena such as the tidal locking of celestial bodies.**

***Keywords*—semi-analytical modeling; boundary element methods; viscoelasticity; energy dissipation.**

I. Modeling technique

Novel computational approaches modeling the viscoelastic rolling behavior of cylinders and spheres were presented in recent works. e.g. [1]–[6]. In this paper, we build on and extend these methods to model the steady-state spinning behavior of a circular viscoelastic coating under the effect of gravity.

A. Problem setting

Figure 1 shows a rigid cylinder of radius r_i coated with a viscoelastic layer of uniform thickness $t = r_o - r_i$. The coating is perfectly bonded to the cylinder and the system is spinning clockwise at a constant angular speed Ω about its fixed axis at point O. Gravity is acting downwards, i.e. in the direction of the fixed y-axis.

The rectangular coordinate system Oxy is fixed. It is associated with a system of polar coordinates r and θ by means of the usual relations

$$x = r\cos(\theta); \qquad y = r\sin(\theta). \tag{1}$$

The rectangular coordinate system $Ox'y'$ follows the cylinder as it rotates about the fixed point O. It is associated with a system of polar coordinates r' and θ' in a similar way, i.e.

$$x' = r'\cos(\theta'); \qquad y' = r'\sin(\theta'). \tag{2}$$

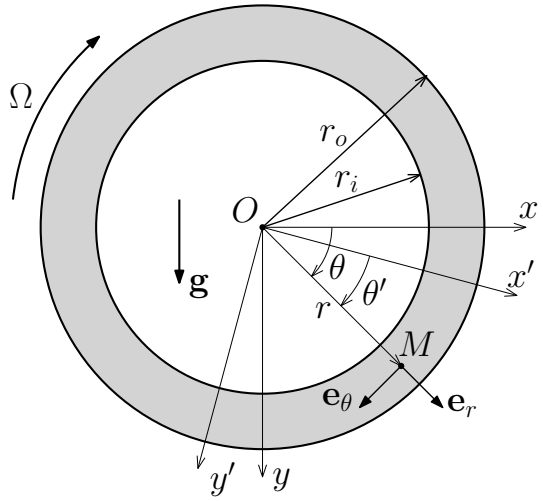

Fig. 1. General model of a coated cylinder and its coordinate systems.

The polar coordinates r and θ of the fixed system can be related to their primed counterparts in the rotating system by a simple transformation involving the time variable t, i.e.

$$r = r'; \qquad \theta = \theta' + \Omega t. \tag{3}$$

Because the state of motion is steady, any generic field $f(r,\theta)$ in the continuum of the coating does not depend explicitly on time. Furthermore, equations (3) lead to a spatial expression of the n^{th}-order derivative of $f(r,\theta)$ with respect to time

$$\frac{d^n f}{dt^n} = \Omega^n \frac{\partial f}{\partial \theta}. \tag{4}$$

.

B. Governing equations

Let u_r and u_θ be the components of the displacement field in $Or\theta$, along the unit vectors $\mathbf{e}_r$ and $\mathbf{e}_\theta$ respectively. The position vector of a (displaced) point $M(r,\theta)$ in the continuum writes

$$\mathbf{x}(r,\theta) = (r + u_r)\,\mathbf{e}_r + u_\theta \mathbf{e}_\theta. \tag{5}$$

The velocity and acceleration fields are obtained by differentiating equation (5) with respect to time, according to expression (4), which yields

$$\mathbf{v}(r,\theta) = \Omega\left[(u_{r,\theta} - u_\theta)\,\mathbf{e}_r + (u_{\theta,\theta} + r + u_r)\,\mathbf{e}_\theta\right], \tag{6}$$

$$\mathbf{a}(r,\theta) = \Omega^2 \left[\left(u_{r,\theta\theta} - 2u_{\theta,\theta} - (r+u_r) \right) \mathbf{e}_r + \left(u_{\theta,\theta\theta} + 2u_{r,\theta} - u_\theta \right) \mathbf{e}_\theta \right]. \quad (7)$$

The local equilibrium equations in the continuum of the layer write

$$\mathbf{div}(\boldsymbol{\sigma}) + \rho\mathbf{g} = \rho\mathbf{a}, \quad (8)$$

where $\boldsymbol{\sigma}$ is the stress tensor, ρ is the density of the viscoelastic material and $\mathbf{g}$ denotes the acceleration of gravity. Plugging equation (7) into (8) and expressing (8) in polar coordinates yields

$$\sigma_{rr,r} + \frac{1}{r}\sigma_{r\theta,\theta} + \frac{1}{r}(\sigma_{rr} - \sigma_{\theta\theta}) + \rho g \sin(\theta) = \rho\Omega^2 \left(u_{r,\theta\theta} - 2u_{\theta,\theta} - (r+u_r) \right), \quad (9a)$$

$$\sigma_{r\theta,r} + \frac{1}{r}\sigma_{\theta\theta,\theta} + \frac{2}{r}\sigma_{r\theta} + \rho g \cos(\theta) = \rho\Omega^2 \left(u_{\theta,\theta\theta} + 2u_{r,\theta} - u_\theta \right). \quad (9b)$$

The term $\rho\Omega^2 r$ appearing in equation (9a) corresponds to the Coriolis effect, which is due to the rotation of the cylinder. The components of the strain tensor $\boldsymbol{\epsilon}$ are expressed, in polar coordinates, in terms of the displacements as follows

$$\epsilon_{rr} = u_{r,r}, \quad (10a)$$

$$\epsilon_{\theta\theta} = \frac{1}{r}\left(u_{\theta,\theta} + u_r \right), \quad (10b)$$

$$\epsilon_{r\theta} = \frac{1}{2}\left(\frac{1}{r}u_{r,\theta} + u_{\theta,r} - \frac{1}{r}u_\theta \right). \quad (10c)$$

Let $\lambda(t)$ and $\mu(t)$ be the time-dependent Lamé parameters characterizing the viscoelastic behavior of the layer's material. Assuming that stresses and strains are equal to zero for all negative values of the time variable t, the constitutive equations of linear isotropic viscoelasticity can be written, using indicial tensor notation, as ([7]–[9])

$$\sigma_{ij}(t) = \int_{-\infty}^{\infty} 2\mu(t-\tau)\frac{\partial\epsilon_{ij}}{\partial\tau}d\tau + \delta_{ij}\int_{-\infty}^{\infty}\lambda(t-\tau)\frac{\partial\epsilon_{kk}}{\partial\tau}d\tau. \quad (11)$$

C. Boundary conditions

The displacement field $\mathbf{u}(r_i,\theta)$ is equal to zero over the inner boundary of the coating, which is attached to the rigid cylinder. Also, the surface tractions $\sigma_{rr}(r_o,\theta)$ and $\sigma_{r\theta}(r_o,\theta)$ are equal to zero over the outer boundary of the coating.

D. Typical Fourier series expansions

The problem setting is spatially periodic in the circumferential direction. Since the rolling takes places in steady-state, any generic field $f(r,\theta)$ in the continuum of the coating is periodic, of periods 2π, in the spatial variable θ. A Fourier series expansion of f writes

$$f(r,\theta) = \sum_{m=-\infty}^{\infty} f_m(r)\, e^{im\theta}, \quad (12)$$

where the Fourier coefficients $f_m(r)$ are given by

$$f_m(r) = \frac{1}{2\pi}\int_{-\pi}^{\pi} f(r,\theta)\, e^{-im\theta}d\theta. \quad (13)$$

Equations (12) and (13) are applied to the stresses, displacements and strains in the viscoelastic coating.

E. General solution to Fourier coefficients

Both sets of equations (9) and (10) can be expressed in terms of Fourier coefficients by substituting relevant fields by their Fourier series expansions (i.e equation (12)) and using the orthogonality property of complex exponentials. In the domain of Fourier coefficients, the equilibrium equations write

$$\dot{\sigma}_{rr_m} + \frac{1}{r}(\sigma_{rr_m} - \sigma_{\theta\theta_m}) + \frac{im}{r}\sigma_{r\theta_m} + \frac{i\rho g}{2}(\delta_{-1m} - \delta_{1m}) + \rho\Omega^2\left(\left(1+m^2\right)u_{r_m} + 2imu_{\theta_m} + r\delta_{m0} \right) = 0, \quad (14a)$$

$$\dot{\sigma}_{r\theta_m} + \frac{im}{r}\sigma_{\theta\theta_m} + \frac{2}{r}\sigma_{r\theta_m} + \frac{\rho g}{2}(\delta_{-1m} + \delta_{1m}) - \rho\Omega^2\left(2imu_{r_m} - \left(1+m^2\right)u_{\theta_m} \right) = 0, \quad (14b)$$

where δ_{ij} is the Kronecker delta and the upper dot ($\dot{}$) denotes differentiation with respect to the spatial variable r. The strain equations in (10) are transformed into the Fourier domain, similarly, which yields

$$\epsilon_{rr_m} = \dot{u}_{r_m}, \quad (15a)$$

$$\epsilon_{\theta\theta_m} = \frac{1}{r}\left(imu_{\theta_m} + u_{r_m} \right), \quad (15b)$$

$$\epsilon_{r\theta_m} = \frac{1}{2}\left(\frac{im}{r}u_{r_m} + \dot{u}_{\theta_m} - \frac{1}{r}u_{\theta_m} \right). \quad (15c)$$

The constitutive equations are handled as follows: Fourier series expansions (12) of stresses and strains are plugged into equation (11) and all terms in the latter are shifted to the left-hand-side. Equation (3) is then used to reveal the time variable explicitly

$$\sum_{m=-\infty}^{\infty}\sigma_{ij_m}(r)\, e^{im\theta'}e^{im\Omega t} - \int_{-\infty}^{\infty} 2\mu(t-\tau)\frac{\partial}{\partial\tau}\left(\sum_{m=-\infty}^{\infty}\epsilon_{ij_m}(r)\, e^{im\theta'}e^{im\Omega\tau} \right)d\tau - \delta_{ij}\int_{-\infty}^{\infty}\lambda(t-\tau)\frac{\partial}{\partial\tau}\left(\sum_{m=-\infty}^{\infty}\epsilon_{kk_m}(r)\, e^{im\theta'}e^{im\Omega\tau} \right)d\tau = 0. \quad (16)$$

Partial differentiation with respect to time is performed and terms are rearranged under the same summation sign so that the complex exponential in θ' can be factored out. The orthogonality of complex exponentials is then invoked to eliminate the summation sign, which yields

$$\sigma_{ij_m}(r)\, e^{im\Omega t} - im\Omega\int_{-\infty}^{\infty} 2\mu(t-\tau)\, e^{im\Omega\tau}d\tau\epsilon_{ij_m}(r) - \delta_{ij}im\Omega\int_{-\infty}^{\infty}\lambda(t-\tau)\, e^{im\Omega\tau}d\tau\epsilon_{kk_m}(r) = 0. \quad (17)$$

The change of variable $\xi = t - \tau$ is then introduced, and the complex exponential in the variable t is factored out

$$\left[\sigma_{ij_m}(r) - im\Omega \int_{-\infty}^{\infty} 2\mu(\xi)\, e^{-im\Omega\xi} d\xi \epsilon_{ij_m}(r) - \delta_{ij} im\Omega \int_{-\infty}^{\infty} \lambda(\xi)\, e^{-im\Omega\xi} d\xi \epsilon_{kk_m}(r)\right] e^{im\Omega t} = 0. \quad (18)$$

The above being true for all times t, it may be concluded that

$$\sigma_{ij_m}(r) = 2\mu_m^* \epsilon_{ij_m}(r) + \lambda_m^* \epsilon_{kk_m}(r)\, \delta_{ij}, \quad (19)$$

where $\omega_m = m\Omega$, $\mu_m^* = \mu^*(\omega_m) = i\omega_m \hat{\mu}(\omega_m)$, $\lambda_m^* = \lambda^*(\omega_m) = i\omega_m \hat{\lambda}(\omega_m)$, $\hat{\mu}(\omega_m)$ and $\hat{\lambda}(\omega_m)$ being the Fourier transforms of $\mu(t)$ and $\lambda(t)$, respectively.

After all governing equations have been transformed into the domain of Fourier coefficients, four state variables are retained and arranged is a state vector $\mathbf{q}_m$ as indicated below

$$\mathbf{q}_m(r) = \langle \mathbf{d}_m(r), \mathbf{f}_m(r) \rangle^T, \quad (20)$$

where

$$\mathbf{d}_m(r) = \langle u_{r_m}(r), u_{\theta_m}(r) \rangle^T,$$
$$\mathbf{f}_m(r) = \langle \sigma_{rr_m}(r), \sigma_{r\theta_m}(r) \rangle^T.$$

Combining equations (14), (15) and (19), and eliminating non-state quantities yields the following system of ordinary differential equations in the state variables

$$\dot{u}_{r_m} = -\frac{\lambda_m^* \mathcal{S}_{1_m}^*}{r}\left(u_{r_m} + imu_{\theta_m}\right) + \mathcal{S}_{1_m}^* \sigma_{rr_m}, \quad (21a)$$

$$\dot{u}_{\theta_m} = -\frac{im}{r} u_{r_m} + \frac{1}{r} u_{\theta_m} + \frac{1}{\mu_m^*} \sigma_{r\theta_m}, \quad (21b)$$

$$\dot{\sigma}_{rr_m} = \left(\frac{\mathcal{S}_{2_m}^*}{r^2} - \rho\Omega^2\left(1 + m^2\right)\right) u_{r_m} + im\left(\frac{\mathcal{S}_{2_m}^*}{r^2} - 2\rho\Omega^2\right) u_{\theta_m} - \frac{2\mu_m^* \mathcal{S}_{1_m}^*}{r} \sigma_{rr_m} - \frac{im}{r} \sigma_{r\theta_m} - \rho\Omega^2 r \delta_{m0} - \frac{i\rho g}{2}\left(\delta_{-1m} - \delta_{1m}\right), \quad (21c)$$

$$\dot{\sigma}_{r\theta_m} = -im\left(\frac{\mathcal{S}_{2_m}^*}{r^2} - 2\rho\Omega^2\right) u_{r_m} + \left(\frac{\mathcal{S}_{2_m}^*}{r^2} m^2 - \rho\Omega^2\left(1 + m^2\right)\right) u_{\theta_m} - im\frac{\lambda_m^* \mathcal{S}_{1_m}^*}{r} \sigma_{rr_m} - \frac{2}{r} \sigma_{r\theta_m} - \frac{\rho g}{2}\left(\delta_{-1m} + \delta_{1m}\right), \quad (21d)$$

where $S_{1_m}^*$ and $S_{2_m}^*$ are shorthand parameters defined below

$$\mathcal{S}_{1_m}^* = 1/\left(\lambda_m^* + 2\mu_m^*\right), \quad (22a)$$

$$\mathcal{S}_{2_m}^* = 4\mu_m^*\left(\lambda_m^* + \mu_m^*\right)\mathcal{S}_{1_m}^*. \quad (22b)$$

By analogy to forced time-varying systems in linear system theory (e.g. [10]), equations (21) can be written in the form

$$\dot{\mathbf{q}}_m(r) = \mathbf{A}_m(r)\, \mathbf{q}_m(r) + \mathbf{b}_m(r) \quad (23)$$

where $\mathbf{A}_m(r)$ is a 4×4 complex-valued matrix and the 'forcing' term $\mathbf{b}_m(r)$, resulting from gravity and the Coriolis effect, writes

$$\mathbf{b}_m(r) = \left\langle 0, 0, -\rho\Omega^2 r\delta_{m0} - \frac{i\rho g}{2}\left(\delta_{-1m} - \delta_{1m}\right), -\frac{\rho g}{2}\left(\delta_{-1m} + \delta_{1m}\right)\right\rangle^T. \quad (24)$$

The solution to system (23) is of the form

$$\mathbf{q}_m(r) = \mathbf{T}_m(r, r_i)\, \mathbf{q}_m(r_i) + \mathbf{J}_m(r, r_i), \quad (25)$$

where $\mathbf{J}_m(r, r_i)$ is given by

$$\mathbf{J}_m(r, r_i) = \int_{r_i}^{r} \mathbf{T}_m(r, s)\, \mathbf{b}_m(s)\, ds, \quad (26)$$

and $\mathbf{T}_m(r, r_i)$ corresponds to the state-transition matrix. Equation (25) can be written in the form

$$\begin{bmatrix} \mathbf{d}_m(r) \\ \mathbf{f}_m(r) \end{bmatrix} = \begin{bmatrix} \mathbf{T}_{m,11}(r, r_i) & \mathbf{T}_{m,12}(r, r_i) \\ \mathbf{T}_{m,21}(r, r_i) & \mathbf{T}_{m,22}(r, r_i) \end{bmatrix} \times \begin{bmatrix} \mathbf{d}_m(r_i) \\ \mathbf{f}_m(r_i) \end{bmatrix} + \begin{bmatrix} \mathbf{J}_m(r, r_i)(1:2) \\ \mathbf{J}_m(r, r_i)(3:4) \end{bmatrix}, \quad (27)$$

where $\mathbf{J}_m(r, r_i)(p:q)$ denotes the subvector of $\mathbf{J}_m(r, r_i)$ comprising its components p through q. Incorporating the boundary conditions $\mathbf{d}_m(r_i) = \mathbf{0}$, Fourier coefficients of displacements and stresses at r are related explicitly

$$\mathbf{d}_m(r) = \mathbf{T}_{m,12}(r, r_i)\mathbf{T}_{m,22}^{-1}(r, r_i)\left(\mathbf{f}_m(r) - \mathbf{J}_m(r, r_i)(3:4)\right) + \mathbf{J}_m(r, r_i)(1:2). \quad (28)$$

The evaluation of $\mathbf{T}_m(r, r_i)$ can be carried out numerically, to the desired degree of accuracy, using the block-pulse technique proposed in [11]. As a more efficient and straightforward alternative, the integration domain $[r_i, r]$ is divided into n_r sub-intervals of equal size $\Delta r = (r_o - r)/n_r$, and the state-transition matrix $\mathbf{T}_m(r, r_i)$ is written as

$$\mathbf{T}_m(r, r_i) = \prod_{k=1}^{n_r} \mathbf{e}^{\Delta r \mathbf{A}_k}, \quad (29)$$

where $\mathbf{A}_k = \mathbf{A}_m(r_i + (k - \alpha)\Delta r)$, with α chosen in $[0, 1]$. Evaluating expression (26) requires numerical integration, which is computationally expensive. Fortunately, no more than two evaluations are needed in the present case since $\mathbf{b}_m \neq \mathbf{0}$, and hence $\mathbf{J}_m(r, r_i) \neq \mathbf{0}$ for $m \in \{0, \pm 1\}$, only. Plugging equation (28) for the Fourier coefficients $\mathbf{d}_m(r_o)$ into equation (12), it is readily shown that the total displacement field at the outer boundary of the coating $\mathbf{u}(r_o, \theta)$ corresponds to the sum of three terms: $\mathbf{u}^f(r_o, \theta)$ generated by potential surface tractions, $\mathbf{u}^g(r_o, \theta)$ due to gravity and $\mathbf{u}^c(r_o)$ which results from the Coriolis effect. These three terms are given below:

$$\mathbf{u}^f(r_o, \theta) = \sum_{m=-\infty}^{\infty} \left[\mathbf{T}_{m,12}(r_o, r_i)\mathbf{T}_{m,22}^{-1}(r_o, r_i)\mathbf{f}_m(r_o)\, e^{im\theta}\right], \quad (30a)$$

$$\mathbf{u}^g(r_o, \theta) = 2\Re\left[\mathbf{J}_1(r_o, r_i)(1:2) - \mathbf{T}_{1,12}(r_o, r_i)\mathbf{T}_{1,22}^{-1}(r_o, r_i)\mathbf{J}_1(r_o, r_i)(3:4)e^{i\theta}\right], \quad (30b)$$

$$\mathbf{u}^c(r_o) = \mathbf{J}_0(r_o, r_i)(1:2) - \mathbf{T}_{0,12}(r_o, r_i)\mathbf{T}_{0,22}^{-1}(r_o, r_i)\mathbf{J}_0(r_o, r_i)(3:4). \quad (30c)$$

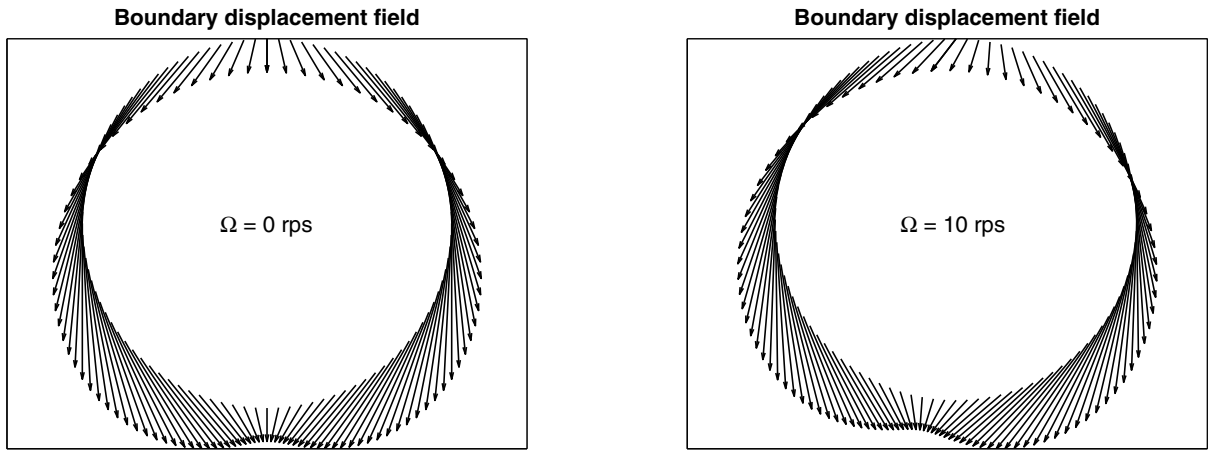

(a) $\Omega = 0$ rps. (b) $\Omega = 10$ rps.

Fig. 2. Quiver plot of the displacement field of the outer boundary of the viscoelastic coating (a) at rest and (b) at an angular speed of $\Omega = 10$ rps. A purely elastic coating would behave as in (a), regardless of the angular speed.

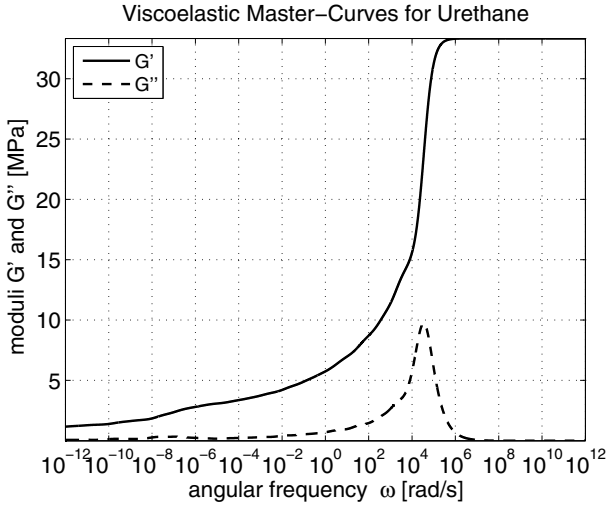

Fig. 3. Frequency-domain master-curves of the Urethane rubber coating.

F. Influence of gravity loads

A compliance matrix reflecting the mechanical behavior of the coating's outer boundary when subjected to surface tractions – characterized by Fourier coefficients $f_m(r_o)$ – can be constructed by performing the synthesis of the Fourier coefficients for the corresponding displacements, as outlined in equation (30a). However, in this work, we focus on studying the behavior of the viscoelastic coating under the influence of gravity, which is reflected by equation (30b).

II. Application model

A rigid cylinder of 10 mm radius coated with a 5 mm thick layer of Urethane rubber and spinning at constant angular speed Ω is retained. The Urethane rubber is characterized by the viscoelastic frequency-domain master-curves shown in Figure 3. These correspond to (i) the storage modulus $G'(\omega)$, which mainly characterizes the variations of material stiffness with the angular frequency ω, and (ii) the loss modulus $G''(\omega)$ which mainly reflects the dependence on ω of the amount of dissipated energy in the bulk.

III. Results and discussion

Figure 2a shows a quiver plot of the displacement field of the outer boundary of the viscoelastic coating at rest, i.e. for $\Omega = 0$ rps. It is interesting to note that, had the coating been purely elastic, its time-independent response would have also resulted in the displacement field shown in Figure 2a, regardless of the angular speed Ω.

Figure 2b shows a quiver plot of the same field when the cylinder is spinning clockwise, in steady-state, at an angular speed $\Omega = 10$ rps. In these conditions, the center of gravity of the coating material is clearly shifted to the left – as compared to the case of Figure 2a – which induces a counterclockwise moment about the axis of rotation, due to gravity. This resisting torque opposes the spinning motion and would slow the cylinder down in the absence of a balancing driving torque maintaining the speed.

Excluding any potential losses of power due to friction in the mechanisms involved, it is interesting to note that maintaining the system in steady-state motion under the influence of a force field, such as that due to gravity, requires the sustained provision of energy. This energy is dissipated in the bulk of the viscoelastic material where it is transformed into heat.

The variations of the magnitude of the displacement field with the angular coordinate θ over the outer boundary of the viscoelastic coating are shown in Figure 4, for different values of the angular speed $\Omega = 0$, 1.10^{-10}, 1.10^{-5}, and 10 rps. The angle θ increases clockwise and the value $\theta = \pi/2$ corresponds to the vertical axis pointing in the direction of the gravity loads. Both axes in Figure 4 are reversed to be

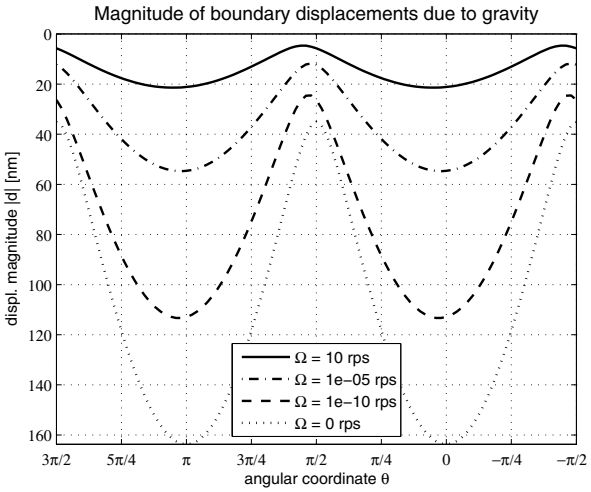

Fig. 4. Variations of the displacement field magnitude over the outer boundary of the viscoelastic coating with the angular coordinate θ, for different values of the angular speed Ω.

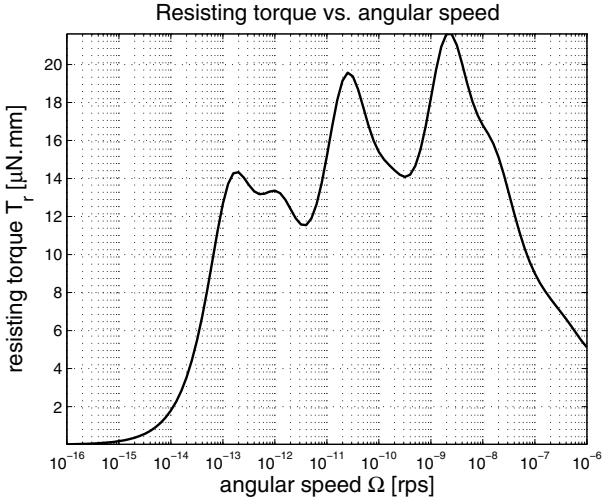

Fig. 5. Variations of the viscoelastic resisting torque with the angular speed.

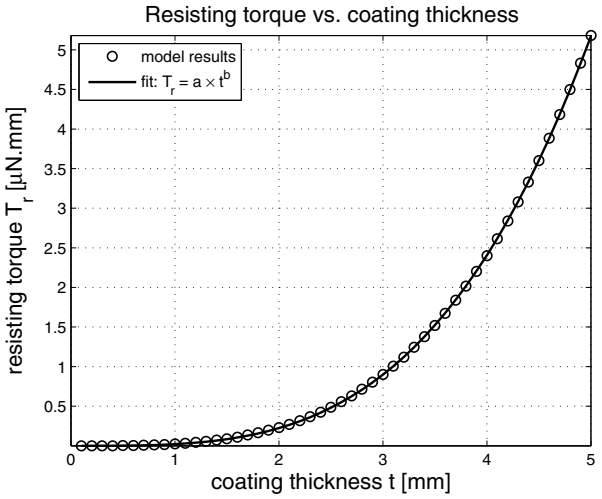

Fig. 6. Variations of the viscoelastic resisting torque with coating thickness, for $r_i = 10$ mm and $\Omega = 10$ rps.

consistent with the results displayed in Figure 2 and thus improve its readability. The curves in Figure 4 are clearly shifted to the left and decrease in amplitude as the angular speed Ω increases. The reduction in amplitude is mainly due to the fact that the storage modulus $G'(\omega)$, i.e. the material stiffness, increases with frequency (see Figure 3). The lateral shift to the left of the material that constitutes the viscoelastic coating results in an eccentricity of the weight which causes the dissipative torque $T_r(\Omega)$ acting counterclockwise and thus resisting the motion (for $\Omega > 0$).

The variations of the viscoelastic resisting torque T_r with the angular speed Ω are shown in Figure 5, for this application example. In general, the curve $T_r(\Omega)$ depends on the geometry – i.e. inner and outer radius of the coating – and on the material parameters retained, i.e. $G'(\omega)$ and $G''(\omega)$. Linear viscoelastic solid material models can be conceptually represented by arrangements of ideal springs and dashpots. When such models are subjected to relatively low rates of deformation, the dashpots flow and oppose little resistance to motion. Also, under relatively high deformation rates, the dashpots block and act as perfectly rigid connections. Thus, in both extremes cases $\Omega \to 0$ and $\Omega \to \infty$, the material model reduces to an arrangement of ideal springs and thus behaves as if it were purely elastic. One thus expects that the resisting torque will decrease on the left and on the right in Figure 5, which is indeed the case. In the particular case presented here the behavior is characterized by three main peaks (roughly 14.3, 19.6 and 21.6 μN.mm) of energy dissipation at intermediate angular speeds ($2\ 10^{-13}$, $2.5\ 10^{-11}$, and $2\ 10^{-9}$ rps, respectively).

The resisting torque T_r also varies with the thickness t of the coating. This is shown in Figure 6, for a cylinder radius $r_i = 10$ mm at an angular speed $\Omega = 10$ rps. It is clear that T_r increases with t following a trend that it well fitted by a power law $T_r = a \times t^b$ where $a = 0.2083$ (95% C.I. $[0.2066, 0.2101]$) and $b = 3.4261$ (95% C.I. $[3.4206, 3.4317]$).

Retaining a fixed value $r_o = 15$ mm for the outer radius of the coating, the inner radius (i.e. the radius of the rigid cylinder) is varied between zero and r_o and the curve $T_r(r_i)$ is plotted in Figure 7, for an angular velocity $\Omega = 10$ rps. It is interesting to note that: (i) as r_i becomes close to zero (on the left), the resisting torque tends towards a maximum value which corresponds to the limiting case of a plain viscoelastic cylinder, and (ii) as r_i approaches r_o (on the right) the viscoelastic coating becomes extremely thin and thus the resisting torque tends to zero. The model's data points are well fitted by an analytical expression of the form

$$T_r(r_i) = (r_o - r_i)^a \left(e^{(-br_i^c)} + e^{(-dr_i^e)} \right), \qquad (31)$$

where the five parameters take the following values, with their 95% confidence intervals: $a = 2.027\,[2.025, 2.029]$, $b = 0.2842\,[0.2658, 0.3026]$, $c = 0.7078\,[0.6605, 0.7552]$,

$d = 3.667\,[3.425, 3.909]$, $e = 0.6416\,[0.6173, 0.6659]$.

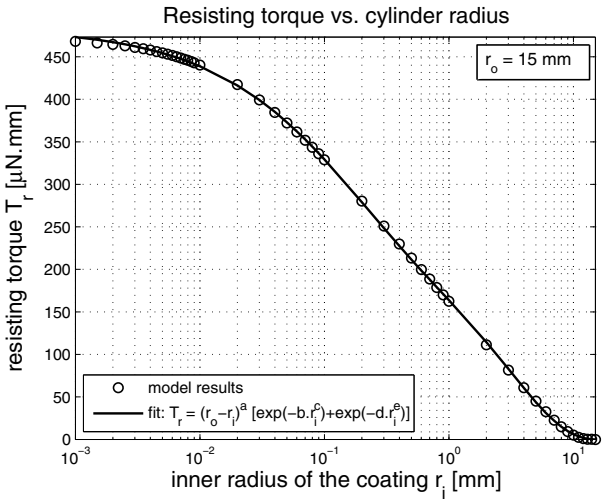

Fig. 7. Variations of the resisting torque T_r with the inner radius r_i of the viscoelastic coating, for $r_o = 15$ mm and $\Omega = 10$ rps.

IV. Conclusion

It might be interesting to explore the conditions – mainly the orders of magnitude of the parameters – under which a curve such as $T_r\,(\Omega)$, determined experimentally, can be inverted to characterize the viscoelastic material of which the coating is made, i.e. to determine $G'\,(\omega)$ and $G''\,(\omega)$.

The application example presented here is also strongly reminiscent of the phenomenon corresponding to the formation of tides generating tidal torques that result in the tidal locking of celestial bodies (see e.g. [12]–[20]). For instance, the reason that we always see only one side of the moon is that it is tidally locked to Earth. The semi-analytical computational approach presented in this manuscript can be extended to model aspects of the behavior of celestial bodies and possibly determine, from remote observation, the materials of which these are composed.

The model could also be used to study the behavior of viscoelastic cylinders under gravitational loads such as optical resonators in precision measurement devices (e.g. [21]) or solid propellant grains (e.g. [22]–[25]).

References

[1] X. Qiu, "Full two-dimensional model for rolling resistance: hard cylinder on viscoelastic foundation of finite thickness," *Journal of Engineering Mechanics*, vol. 132, no. 11, pp. 1241–1251, 2006.

[2] ——, "Full two-dimensional model for rolling resistance. ii: Viscoelastic cylinders on rigid ground," *Journal of Engineering Mechanics*, vol. 135, no. 1, pp. 20–30, 2009.

[3] G.-P. Zéhil and H. P. Gavin, "Three-dimensional boundary element formulation of a viscoelastic layer of finite thickness applied to the rolling resistance of a rigid sphere," *International Journal of Solids and Structures*, vol. 50, no. 6, pp. 833–842, 2013. [Online]. Available: http://www.sciencedirect.com/science/article/pii/S002076831200491X

[4] ——, "Simplified approaches to viscoelastic rolling resistance," *International Journal of Solids and Structures*, vol. 50, no. 6, pp. 853–862, 2013. [Online]. Available: http://www.sciencedirect.com/science/article/pii/S002076831200409X

[5] ——, "Two and three-dimensional boundary element formulations of compressible isotropic, transversely isotropic and orthotropic viscoelastic layers of arbitrary thickness, applied to the rolling resistance of rigid cylinders and spheres," *European Journal of Mechanics - A/Solids*, vol. 44, pp. 175–187, 2014. [Online]. Available: http://www.sciencedirect.com/science/article/pii/S0997753813001289

[6] ——, "Rolling resistance of a rigid sphere with viscoelastic coatings," *International Journal of Solids and Structures*, vol. 51, no. 3-4, pp. 822–838, 2014. [Online]. Available: http://www.sciencedirect.com/science/article/pii/S0020768313004447

[7] W. Flügge, *Viscoelasticity*. Springer-Verlag, 1975.

[8] R. Lakes, *Viscoelastic Materials*. Cambridge University Press, 2009.

[9] N. Tschoegl, *The phenomenological theory of linear viscoelastic behavior: an introduction*. Springer-Verlag, 1989.

[10] J. Lygeros and F. Ramponi, *Lecture notes on linear system theory*. Automatic Control Laboratory, ETH Zurich, 2010. [Online]. Available: http://control.ee.ethz.ch/ ifalst/docs/Notes/LectureNotes.pdf

[11] B. Rammohan Rao and S. Ganapathy, "Linear time-varying systemsstate transition matrix," *Electrical Engineers, Proceedings of the Institution of*, vol. 126, no. 12, pp. 1331–1335, 1979.

[12] Y. V. Barkin and V. G. Vilke, "Celestial mechanics of planet shells," *Astronomical & Astrophysical Transactions*, vol. 23, no. 6, pp. 533–553, 2004. [Online]. Available: http://dx.doi.org/10.1080/10556790412331319668

[13] V. V. Bondarenko, Y. G. Markov, A. M. Mikisha, L. V. Rykhlova, and I. V. Skorobogatykh, "Gravitationaltidal evolution of planetary subsystems of the sun," *Astronomical and Astrophysical Transactions*, vol. 25, no. 4, pp. 275–290, 2006. [Online]. Available: http://dx.doi.org/10.1080/10556790600960697

[14] J. Laskar, G. Boué, and A. C. M. Correia, "Tidal dissipation in multi-planet systems and constraints on orbit fitting," *A&A*, vol. 538, p. A105, 2012. [Online]. Available: http://dx.doi.org/10.1051/0004-6361/201116643

[15] S. J. PEALE, "Contribution of tidal dissipation to lunar thermal history," *Icarus*, vol. 36, pp. 245–269, 1978.

[16] S. K. Poulsen, "Tidal deformation of the solid earth – a finite difference discretization," March 2009.

[17] Remus, F., Mathis, S., and Zahn, J.-P., "The equilibrium tide in stars and giant planets," *A&A*, vol. 544, p. A132, 2012. [Online]. Available: http://dx.doi.org/10.1051/0004-6361/201118160

[18] M. Ross and G. Schubert, "Tidal dissipation in a viscoelastic planet," *Journal of Geophysical Research - Proceedings of the sixteenth lunar and planatary science conference - Part 2*, vol. 91, no. B4, pp. D447–D452, 1986.

[19] G. Tobie, A. Mocquet, and C. Sotin, "Tidal dissipation within large icy satellites: Applications to europa and titan," *Icarus*, vol. 177, no. 2, pp. 534 – 549, 2005, europa Icy Shell. [Online]. Available: http://www.sciencedirect.com/science/article/pii/S0019103505001582

[20] W. E. VanArsdale, "Orbital dynamics of a viscoelastic body," *Journal of Geophysical Research: Solid Earth*, vol. 90, no. B8, pp. 6887–6892, 1985. [Online]. Available: http://dx.doi.org/10.1029/JB090iB08p06887

[21] S. Scheithauer and C. Lmmerzahl, "Analytical solution for the deformation of a cylinder under tidal gravitational forces," *Classical and Quantum Gravity*, vol. 23, no. 24, p. 7273, 2006. [Online]. Available: http://stacks.iop.org/0264-9381/23/i=24/a=006

[22] V. A. Bunakov, "Deformations of a thick-valued, slowly rotating cylinder under gravitational load," *Mekhanika Polimerov*, vol. 4, pp. 727–733, 1970.

[23] ——, "Viscoelastic deformations of a thick-walled cylinder under prolonged exposure to gravitational stresses," *Mekhanika Polimerov*, vol. 5, pp. 846–853, 1972.

[24] G. Lianis, "Stresses and strains in solid propellants during storage," *ARS Journal*, vol. 32, no. 5, pp. 688–692, 1962.

[25] M. L. Williams, "The strain analysis of solid propellant rocket grains," *Journal of the Aerospace Sciences*, vol. 27, no. 8, pp. 574–586, 1960.